Sol−Gel Processing of Semiconducting Metal Chalcogenide Xerogels: Influence of Dimensionality on Quantum Confinement Effects in a Nanoparticle Network

Indika U. Arachchige, Jaya L. Mohanan, and Stephanie L. Brock*

Department of Chemistry, Wayne State University, Detroit, Michigan 48202

Received August 15, 2005

The synthesis and characterization of porous nanostructured inorganic polymers (gels and xerogels) of CdS, ZnS, PbS, and CdSe is described. Primary particles are synthesized via water-in-oil microemulsions, surface complexed with thiolate ligands, and dispersed in acetone. Oxidation of the thiolate ligands with H_2O_2 leads to particle aggregation and the formation of wet gels, which are then dried under ambient conditions to produce xerogels. The xerogels exhibit optical band-edges that are intermediate between bulk precipitates and the more porous wet gels and aerogels, suggesting the extent of quantum confinement in such colloidal networks is intimately related to the pore structure and surface area (dimensionality). Heating of the xerogels in vacuo results in a continued decrease in the energy of absorption onset due to sintering of the nanoparticle network, and this is also reflected in a growth in crystallite size as probed by powder X-ray diffraction. The resulting xerogel networks demonstrate modest Brunauer−Emmett−Teller (BET) surface areas of 29−65 m^2/g with Barrett−Joyner−Halenda (BJH) average pore sizes of 3−15 nm, considerably smaller than values obtained for corresponding aerogels and consistent with increased density (decreased dimensionality).

Introduction

Inorganic nanomaterials have become the subject of intense research in recent years due to their unique optical, electronic, and magnetic properties. Accordingly, there have been many reports on the synthesis and characterization of discrete nanoparticles with excellent control of size, shape, and polydispersity. Among these nanomaterials, the 12−16 and 14−16 semiconductors, MQ (M = Cd, Zn, Pb; Q = S, Se, Te), have gained considerable attention from the scientific community due to their size-tunable optical absorption and sharp band-edge luminescence properties.[1,2] Hence, CdS and CdSe nanocrystals are being investigated for applications in nonlinear optics,[3] biological labeling and diagnostics,[4] electroluminescence[5,6] and photovoltaic devices,[7−9] as well as sensors.[10−12] ZnS and PbS nanocrystals have potential applications in photovoltaic and electroluminescence devices (ZnS)[13] as well as in IR detectors and ion-selective sensors (PbS).[14] One remaining challenge for employing nanoparticles in many of these applications is to assemble them into solid-state structures while retaining their unique properties.

Typical construction strategies include self-assembly of colloidal crystals in two or three dimensions[15−17] and the linking together of particles through molecular tethers.[18−20] In these cases, the quantum-confined properties of semiconducting particles are controlled by the separation distance between particles (mandated by the thickness of the organic capping agent and/or the length of the tether) as well as the geometry.[20,21] Recently, we have adopted a sol−gel strategy for the production of metal chalcogenide aerogels, in which nanoparticles are chemically linked to each other, *with no intervening layer*, to create a cross-linked, colloidal polymer in the solid state that retains the unique optical properties of

* To whom correspondence should be addressed: tel 313-577-3102; fax 313-577-8822; e-mail sbrock@chem.wayne.edu.

(1) Alivisatos, A. P. *Science* **1996**, *271*, 933−937.
(2) Wang, Y.; Herron, N. *J. Phys. Chem.* **1991**, *95*, 525−532.
(3) Amore, F. D.; Pietralunga, S. M.; Lorusso, P.; Martinelli, M.; Zappettini, A.; Dal Bo, E.; Tassone, F.; Tognini, P.; Travagnin, M. *Phys. Status Solidi C* **2004**, *4*, 1001−1004.
(4) Michalet, X.; Pinaud, F. F.; Bentolila, L. A.; Tsay, J. M.; Doose, S.; Li, J. J.; Sundaresan, G.; Wu, A. M.; Gambhir, S. S.; Weiss, S. *Science* **2005**, *307*, 538−544.
(5) Colvin, V. L.; Schlamp, M. C.; Alivisatos, A. P. *Nature* **1994**, *370*, 354−357.
(6) Dabbousi, B. O.; Bawendi, M. G.; Onitsuka, O.; Rubner, M. F. *Appl. Phys. Lett.* **1995**, *66*, 1316−1318.
(7) Huynh, W. U.; Dittmer, J. J.; Alivisatos, A. P. *Science* **2002**, *295*, 2425−2427.
(8) Liu, J.; Tanaka, T.; Sivula, K.; Alivisatos, A. P.; Fréchet, J. M. J. *J. Am. Chem. Soc.* **2004**, *126*, 6550−6551.
(9) Sun, B.; Marx, E.; Greenham, N. C. *Nano Lett.* **2003**, *3*, 961−963.
(10) Ivanisevic, A.; Reynolds, M. F.; Burstyn, J. N.; Ellis, A. B. *J. Am. Chem. Soc.* **2000**, *122*, 3731−3738.
(11) Meeker, K.; Ellis, A. B. *J. Phys. Chem. B* **1999**, *103*, 995−1001.
(12) Nazzal, A. Y.; Qu, L.; Peng, X.; Xiao, M. *Nano Lett.* **2003**, *3*, 819−822.
(13) Yang, Y.; Huang, J.; Liu, S.; Shen, J. *J. Mater. Chem.* **1997**, *7*, 131−133.
(14) Wang, W.; Liu, Y.; Zhan, Y.; Zheng, C.; Wang, G. *Mater. Res. Bull.* **2001**, *36*, 1977−1984.
(15) Whetten, R. L.; Shafigullin, M. N.; Khoury, J. T.; Schaaff, T. G.; Vezmar, I.; Alvarez, M. M.; Wilkinson, A. *Acc. Chem. Res.* **1999**, *32*, 397−406.
(16) Redl, R. X.; Cho, K.-S.; Murray, C. B.; O'Brien, S. *Nature* **2003**, *423*, 968−971.
(17) Murray, C. B.; Kagan, C. R.; Bawendi, M. G. *Annu. Rev. Mater. Sci.* **2000**, *30*, 545−610.
(18) Lee, J.; Govorov, A. O.; Dulka, J.; Kotov, N. A. *Nano Lett.* **2004**, *4*, 2323−2330.
(19) Tang, Z.; Kotov, N. A. *Adv. Mater.* **2005**, *17*, 951−962.
(20) Kim, J. Y.; Osterloh, F. E. *J. Am. Chem. Soc.* **2005**, *127*, 10152−10153.
(21) Kagan, C. R.; Murray, C. B.; Bawendi, M. G. *Phys. Rev. B* **1996**, *54*, 8633−8643.

10.1021/cm0518325 CCC: $30.25
Published on Web 11/19/2005

the nanoparticle building blocks.[22,23] We postulate that the quantum confinement effects, noted in both wet gels[24−27] and aerogels,[22,23] arise from the low dimensionality of the network and not from any surface passivation or barriers between the particles. The effect of dimension on the extent of quantum confinement has been a topic of great theoretical and experimental interest, focused largely on systems with well-defined dimensionality (particles, wires, wells) and dimensionality intermediate between 0-D and 1-D (i.e., short rods).[28−33] The gel framework also results in an intermediate dimensionality, only of a more complex (fractal) nature.[34] Thus, the extent of quantum confinement in gels relative to the discrete nanoparticle building blocks should correlate to the surface area and porosity of the system; that is, the formation of a more-dense framework is expected to yield a lesser degree of confinement.

The combination of porosity with quantum confinement effects is expected to yield materials that are superior to discrete nanoparticles and nanoparticle films for applications requiring rapid molecular transport and charge separation, such as sensing,[12,35,36] photocatalysis,[37−40] and composite photovoltaic devices.[7−9,41,42] Unlike discrete quantum dots, a physically linked system should permit the conduction of electrons from dot to dot, without significant hopping or the need to introduce organic linkers or conducting surfactants, as in other systems.[43−46] However, aerogel processing techniques involve supercritical solvent extraction steps to avoid capillary collapse and densification during solvent removal and are therefore difficult to adapt to large volume and/or thin film production. Additionally, for many applications that depend on molecular transport, the extremely low density of the aerogel framework (as little as 1.5% that of a single crystal for the CdS system) is unnecessary. What *is* critical for facile molecular transport is the presence of interconnected pores in the mesoporous (2−50 nm) range, since diffusion rates through 10−50 nm pores approach those of molecules in open air.[47,48]

In this work, we explore the effect of ambient pressure drying on the structure, optical properties and surface area/pore size of metal chalcogenide gels of CdS, ZnS, PbS, and CdSe. These new xerogel materials are compared to corresponding aerogels,[22,23] and the role of framework density on quantum confinement effects in such physically linked 3-D branched nanoparticle arrays is discussed.

Experimental Section

Materials. Bis-(2-ethylhexyl)sulfosuccinate sodium salt (AOT, 96%), cadmium nitrate tetrahydrate (99%), and triethylamine (TEA, 99%) were purchased from Acros. Acetone, 4-fluorobenzenethiol (98%), tetranitromethane, zinc acetate (99.99%), and sodium sulfide were purchased from Aldrich. Sodium selenide (99.8%) was purchased from Alfa-Aesar. Lead nitrate, 3% aqueous hydrogen peroxide, and *n*-heptane were purchased from Fisher. All chemicals were used as received.

Synthesis of CdS Xerogels. The synthetic procedure for CdS nanoparticle synthesis and capping was adapted from Gacoin et al.[24,26] and was conducted under air-free conditions by use of a Schlenk line. Nanoparticles were prepared by use of a water-in-oil microemulsion with a surfactant-to-water ratio of 5 ($W = [AOT]/[H_2O] = 5$). Typical syntheses were conducted as follows: 111.53 g of surfactant (AOT) was dissolved in 477.5 mL of *n*-heptane; the resulting solution was divided in half, and 11.25 mL of 0.15 M $Cd(NO_3)_{2(aq)}$ was added to one portion and 11.25 mL of 0.15 M $Na_2S_{(aq)}$ was added to the other. The resulting microemulsions were vigorously stirred for 45 min until they became optically clear, and then the solution containing AOT/*n*-heptane/$S^{2-}_{(aq)}$ was transferred by cannula into the solution of AOT/ *n*-heptane/$Cd^{2+}_{(aq)}$ to synthesize the CdS nanoparticles. To cap the nanoparticles, 1.8 mL of 4-fluorobenzenethiol and 2.2 mL of triethylamine were added, resulting in a yellow precipitate. After 1 h of stirring, the precipitate was isolated by centrifugation and washed three times with *n*-heptane to remove the AOT surfactant and excess capping agent (4-fluorobenzenethiol). The resulting precipitate was subsequently dispersed in 20 mL of acetone to form the CdS sol.

For gelation, the CdS sol was divided into 2 mL aliquots and 0.1 mL of 3% aqueous H_2O_2 was added to each aliquot. The mixture was shaken vigorously to ensure homogeneous mixing and allowed to sit undisturbed for gelation. In a typical synthesis, gelation was observed 1−2 h after the oxidant was mixed. The resulting gels were aged for 10−14 days under ambient conditions. CdS wet gels were subsequently washed and exchanged with acetone 6−8 times

(22) Mohanan, J. L.; Arachchige, I. U.; Brock, S. L. *Science* **2005**, *307*, 397−400.
(23) Mohanan, J. L.; Brock, S. L. *J. Non-Cryst. Solids* **2004**, *350*, 1−8.
(24) Gacoin, T.; Lahlil, K.; Larregaray, P.; Boilot, J.-P. *J. Phys. Chem. B* **2001**, *105*, 10228−10235.
(25) Gacoin, T.; Malier, L.; Boilot, J.-P. *Chem. Mater.* **1997**, *9*, 1502−1504.
(26) Gacoin, T.; Malier, L.; Boilot, J.-P. *J. Mater. Chem.* **1997**, *7*, 859−860.
(27) Malier, L.; Boilot, J.-P.; Gacoin, T. *J. Sol−Gel Sci. Technol.* **1998**, *13*, 61−64.
(28) Li, J.; Wang, L.-W. *Chem. Mater.* **2004**, *16*, 4012−4015.
(29) Millo, O.; Steiner, D.; Katz, D.; Aharoni, A.; Kan, S.; Mokari, T.; Banin, U. *Physica E* **2005**, *26*, 1−8.
(30) Steiner, D.; Katz, D.; Millo, O.; Aharoni, A.; Kan, S.; Mokari, T.; Banin, U. *Nano Lett.* **2004**, *4*, 1073−1077.
(31) Yoffe, A. D. *Adv. Phys.* **2001**, *50*, 1−208.
(32) Yu, H.; Li, J.; Loomis, R. A.; Gibbons, P. C.; Wang, L.-W.; Buhro, W. E. *J. Am. Chem. Soc.* **2003**, *125*, 16168−16169.
(33) Yu, H.; Li, J.; Loomis, R. A.; Wang, L.-W.; Buhro, W. E. *Nature Mater.* **2003**, *2*, 517−520.
(34) Emmerling, A.; Fricke, J. *J. Non-Cryst. Solids* **1992**, *145*, 113−120.
(35) Murphy, C. J. *Anal. Chem.* **2002**, 520A−5526A.
(36) Fujii, T.; Tanaka, N.; Tai, H.; Obara, S.; Ellis, A. B. *Bull. Chem. Soc. Jpn.* **2000**, *73*, 809−813.
(37) Korgel, B. A.; Monbouquette, H. G. *J. Phys. Chem. B* **1997**, *101*, 5010−5017.
(38) Fujiwara, H.; Hosokawa, H.; Murakoshi, K.; Wada, Y.; Yanagida, S.; Okada, T.; Kobayashi, H. *J. Phys. Chem. B* **1997**, *101*, 8270−8278.
(39) Yin, H.; Wada, Y.; Kitamura, T.; Yanagida, S. *Environ. Sci. Technol.* **2001**, *35*, 227−231.
(40) Hu, J.-S.; Ren, L.-L.; Guo, Y.-G.; Liang, H.-P.; Cao, A.-M.; Wan, L.-J.; Bai, C.-L. *Angew. Chem. Int. Ed.* **2005**, *44*, 1269−1273.
(41) Singh, V. P.; Singh, R. S.; Thompson, G. W.; Jayaraman, V.; Sanagapalli, S.; Rangari, V. K. *Sol. Energy Mater. Sol. Cells* **2004**, *81*, 293−303.
(42) Snaith, H. J.; Whiting, G. L.; Sun, B.; Greenham, N. C.; Huck, W. T. S.; Friend, R. H., *Nano Lett.* **2005**, *5*, 1653−1657.
(43) Guyot-Sionnest, P.; Wang, C. *J. Phys. Chem. B* **2003**, *107*, 7355−7359.
(44) Milliron, D. I.; Alivisatos, A. P.; Pitois, C.; Edder, C.; Fréchet, J. M. J. *Adv. Mater.* **2003**, *15*, 58−61.
(45) Zamborini, F. P.; Leopold, M. C.; Hicks, J. F.; Kulesza, P. J.; Malik, M. A.; Murray, R. W. *J. Am. Chem. Soc.* **2002**, *124*, 8958−8964.
(46) Andres, R. P.; Bielefeld, J. D.; Henderson, J. I.; Janes, D. B.; Kolagunta, V. R.; Kubiak, C. P.; Mahoney, W. J.; Osifchin, R. G. *Science* **1996**, *273*, 1690−1693.
(47) Leventis, N.; Elder, I. A.; Rolison, D. R.; Anderson, M. L.; Merzbacher, C. I. *Chem. Mater.* **1999**, *11*, 2837−2845.
(48) Rolison, D. R. *Science* **2003**, *299*, 1698−1701.

Table 1. Single Crystal Band-Gap Values and UV−Visible/X-ray Powder Diffraction Data for Nanoparticles[a]

sample	bulk band gap (eV)	absorption edge for nanoparticles (eV)	particle size by optical absorption (nm)	crystallite size by PXRD[b] (nm)
PbS	0.37	1.69	4.6	1.7
CdSe	1.74	2.40	4.4	1.9
CdS	2.45	2.86	3.9	1.6
ZnS	3.70	3.99	3.1	1.9

[a] Particle sizes were calculated on the basis of the mass approximation model (UV−visible) and from the Scherrer formula (PXRD). [b] Values were obtained from evaluation of the (111) peak in the PXRD pattern.

over 2 days and dried on the benchtop under ambient conditions to obtain the CdS xerogels.

Synthesis of ZnS and CdSe Xerogels. A synthetic methodology similar to that used for CdS was employed to prepare ZnS and CdSe nanoparticles. Nanoparticles were synthesized in water-in-oil inverse micellar assemblies ($W = 2$), prepared with $Zn(CH_3COO)_2$ or $Cd(NO_3)_2$ (4.5 mL of 0.15 M aqueous solutions) plus AOT and *n*-heptane. In the case of CdSe, Na_2Se (4.5 mL of 0.15 M aqueous solution) was employed instead of Na_2S. The resultant nanoparticles were capped by reaction of 0.72 mL of 4-fluorobenzenethiol and 0.9 mL of triethylamine and dispersed in 20 mL of acetone to form sols of 4-fluorophenylthiolate-capped ZnS and CdSe nanoparticles. Gelation, aging, and drying to yield xerogels of ZnS and CdSe were performed as described for CdS.

Synthesis of PbS Xerogels. PbS nanoparticles were synthesized analogously to the 12−16 nanoparticles ($W = 2$) from aqueous solutions of $Pb(NO_3)_2$ (6.8 mL, 0.15 M) and Na_2S (3.4 mL, 0.15 M) in a 2:1 ratio. Attempts to use a 1:1 volume ratio inevitably led to precipitation rather than colloid formation. The resultant nanoparticles were capped by reaction of 2.4 mL of 4-fluorobenzenethiol and 3.0 mL of triethylamine and dispersed in 30 mL of acetone to form the PbS sol. Gelation, aging, and drying to yield PbS xerogels were performed as described for CdS.

UV−Visible Spectroscopy. Optical absorption measurements of uncapped nanoparticles in *n*-heptane were obtained on a Hewlett-Packard (HP) 8453 spectrophotometer. The nanoparticle microemulsion solutions were diluted 10-fold with *n*-heptane and the diluted solutions were analyzed against an AOT/*n*-heptane blank in the region from 200 to 800 nm.

Diffuse Reflectance UV−Visible Spectroscopy. A Shimadzu model UV-3101PC double-beam, double monochromator spectrophotometer equipped with an integrating sphere was used to measure the optical diffuse reflectance of xerogels. Powdered xerogel samples were evenly spread on a sample holder preloaded with reflectance standard (powdered $BaSO_4$) and measured from 200 to 1760 nm. The reflectance data were converted to absorption,[49,50] and the band edge for each sample was estimated from the intercept of the line extrapolated from the high-energy end of the absorption to the baseline.

Powder X-ray Diffraction. A Rigaku RU 200B X-ray diffractometer with a Cu Kα rotating anode source was used for X-ray powder diffraction measurements. Powdered xerogel samples were deposited on a low background quartz (0001) holder coated with a thin layer of grease. X-ray diffraction patterns were identified by comparison to phases in the International Centre for Diffraction Data (ICDD) powder diffraction file (PDF) database (release 2000).

Energy-Dispersive Spectroscopy. Elemental compositions were obtained from an in situ EDS unit (EDAX Inc.) attached to a Hitachi S-2400 scanning electron microscope (SEM). Xerogel powders were sprinkled on carbon adhesive tabs placed on an aluminum stub, and EDS data were acquired at 25 keV in secondary electron mode.

Surface Area Analysis. A Micromeritics model ASAP 2010 surface area analyzer was used to produce nitrogen physisorption isotherms at 77 K on powdered xerogels. The data were fit to a Brunauer−Emmett−Teller (BET) model to determine the surface areas of the xerogels. The average pore diameter and cumulative pore volumes were calculated with the Barrett−Joyner−Halenda (BJH) model (assuming cylindrical pores) or by a density functional theory (DFT) model (assuming slit-shaped pores). Samples were degassed under vacuum at 100 °C for 48 h prior to the analysis and employed a 30 s equilibrium interval and a 5 mL dose for a total run time of 9−11.5 h (PbS, CdSe, ZnS) or a 50 s equilibrium interval and a 3 mL dose for a total run time of 17.5 h (CdS). Free space values were experimentally determined. Two independently prepared samples were analyzed for each system.

Results and Discussion

Nanoparticle Formation, Gelation, and Xerogel Generation. In our previous work on aerogels, we have demonstrated that the sol−gel methodology for linking nanoparticles together into networks is versatile with respect to both the metal chalcogenide system being investigated and the method by which the nanoparticle precursor is synthesized (the high-temperature method that produces strongly luminescent dots or the room-temperature method that yields weakly luminescent dots).[22,23] As a major focus of the current study is to probe the effect of dimensionality on quantum confinement in gels (assessed by optical absorption, not luminescence) we adopted the more facile, room-temperature method for nanoparticle synthesis. Accordingly, CdS, ZnS, PbS, and CdSe nanoparticles were prepared and transformed into wet gels by a modification of the synthesis developed by Gacoin et al. for wet gels of CdS.[24,26] Nanoparticles were synthesized by standard room-temperature inverse micellar strategies, complexed with 4-fluorophenylthiolate, and redispersed in acetone to form transparent sols of CdS (yellow), ZnS (colorless), PbS (dark brown), and CdSe (orange). These nanoparticles show the expected quantum confinement effect: a blue shift in the absorption spectra with respect to their bulk band gaps. By use of the mass approximation model,[51,52] nanoparticle diameters were all found to be in the range 3−5 nm (calculated from the optical band-edge data, Table 1). Powder X-ray diffraction patterns of nanoparticle precursors indicate the cubic phase is being produced in each case, as expected from this low-temperature synthetic route.[51] Crystallite size determinations with the Scherrer formula (based on peak breadths) yield values significantly smaller than the particle size values obtained by the mass approximation model, <2 nm (Table

(49) Tandon, S. P.; Gupta, J. P. *Phys. Status Solidi* **1970**, *38*, 363−367.
(50) Wendlandt, W. W.; Helcht, H. G. *Chemical Analysis: Reflectance Spectroscopy*; Interscience: New York, 1966; Vol. 21.
(51) Bandaranayake, R. J.; Wen, G. W.; Lin, J. Y.; Jiang, H. X.; Sorensen, C. M. *Appl. Phys. Lett.* **1995**, *67*, 831−833.
(52) Trindale, T. O.; O'Brien, P.; Pickett, N. L. *Chem. Mater.* **2001**, *13*, 3843−3858.

Table 2. Elemental Compositions of As-Prepared Xerogels[a]

sample	atomic ratios
PbS xerogel	Pb:S 49.7:50.3
CdSe xerogel	Cd:Se:S 47.3:43.5:9.2
CdS xerogel	Cd:S 44.2:55.8
ZnS xerogel	Zn:S 44.9:55.1

[a] Determined by semiquantitative EDS acquired in the SEM.

1). This may reflect the relatively poor crystallinity inherent in particles prepared by room-temperature methods[51,53,54] and/or discrepancies between the actual dielectric constant for CdSe nanoparticles (unknown) and the bulk value (employed here in our calculation).[55]

For all systems, the thiolate groups of capped nanoparticles were oxidatively removed over a period of 10−14 days by use of H_2O_2, yielding the disulfide, $F(C_6H_4)S-S(C_6H_4)F$, as the primary byproduct.[24] As surface groups are irreversibly removed from the particles, the particles aggregate, forming a colloidal wet gel network, as previously described by Gacoin et al.[24−26] for CdS. Wet monolithic gels aged for 10−14 days in the mother liquor were exchanged several times with acetone and air-dried under ambient conditions to form the xerogels. Longer aging time increases the firmness of the wet gel but results in a more compact gel due to syneresis (i.e., the expulsion of solvent from the gel body).

The elemental compositions of as-prepared xerogels were investigated by SEM/EDS. Several independently prepared samples were analyzed, with typical results presented in Table 2. Atomic ratios M:S (M = Cd, Zn, Pb) of 1:1.25 for CdS and ZnS xerogels and almost 1:1 for PbS xerogels were obtained. The increased sulfur content over the expected 1:1 ratio for CdS and ZnS is attributed to the presence of residual capping agent (4-fluorophenylthiolate) in the xerogels, indicating that surface group oxidation has not proceeded to completion. Surprisingly, PbS appears to be nearly stoichiometric, which may be due to the fact that successful precursor particle formation was only achieved when Pb was present in excess (2:1 ratio), thus suggesting that the surface may have been Pb-rich prior to passivation with thiolate. For the CdSe xerogels, the ratio of Cd:Se is nearly 1:1 with a slight deficiency on the part of the Se. Analysis of sulfur content suggests nearly 20 mol % 4-fluorophenylthiolate in the CdSe samples, similar to the values estimated for CdS and ZnS.

It is important to note that Gacoin and co-workers[27] have shown for CdS nanoparticles that, if left long enough, oxidation of the ligand groups will go to completion, thereby confirming that the gel structure is formed from direct physical linkages between adjacent particles and not from bridging functional groups. However, the severe compaction that occurs during complete ligand removal (syneresis) results in a dense glasslike material. Hence, we consider incomplete ligand loss, at least during the initial gelation step, to be important for retaining the porosity and the characteristic properties of the individual quantum dot within the wet gel.

(53) Staniæ, V.; Etsell, T. H.; Pierre, A. C.; Mikula, R. J. *Mater. Lett.* **1997**, *31*, 35−38.
(54) Wu, X.; Wang, D.; Yang, S. *J. Colloid Interface Sci.* **2000**, *222*, 37−40.
(55) Pejova, B.; Tanusevski, A.; Grozdanov, I. J. *Solid State Chem.* **2004**, *177*, 4785−4799.

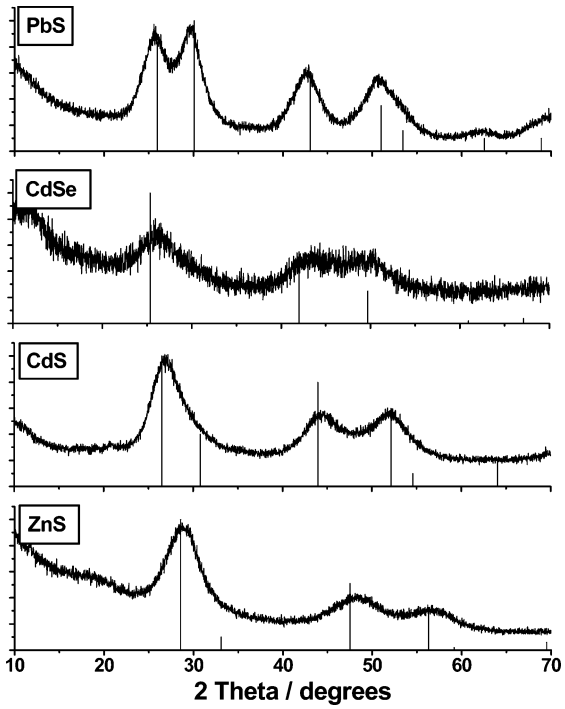

Figure 1. Powder X-ray diffraction patterns of as-prepared PbS, CdSe, CdS, and ZnS xerogels. The ICDD-PDF overlays of cubic PbS (05-0592), CdSe (19-0191), CdS (10-0454), and ZnS (05-0566) are shown as vertical lines.

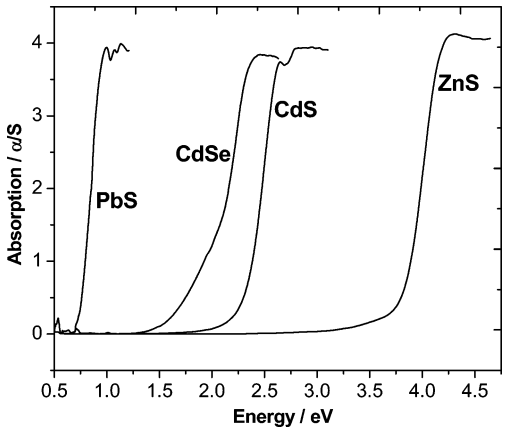

Figure 2. Diffuse reflectance spectra (converted to absorption) of the as-prepared PbS, CdSe, CdS, and ZnS xerogels.

Structure, Optical Properties, and Porosity. Powder X-ray diffraction (PXRD) analysis was used to determine the structure (phase) and the crystallinity of the as-prepared xerogels, as well as samples annealed at 100 °C. PXRD spectra of unannealed PbS, CdSe, CdS, and ZnS xerogels show that the cubic modification observed in the precursor nanoparticles is retained upon gelation in each case (Figure 1). Furthermore, the average crystallite sizes estimated by use of the Scherrer equation (Table 3) have increased only slightly, if at all, during the aggregation, indicating that the formation of a 3-D connected network of nanoparticles occurs without significant crystallite grain growth.

The optical properties of the xerogels were investigated by diffuse reflectance UV−visible spectroscopy. Spectra of as-prepared PbS, CdSe, CdS, and ZnS xerogels are shown in Figure 2. The onsets are generally sharp, similar to what is observed for the discrete nanoparticle precursors; however, the band edge energies have decreased significantly, sug-

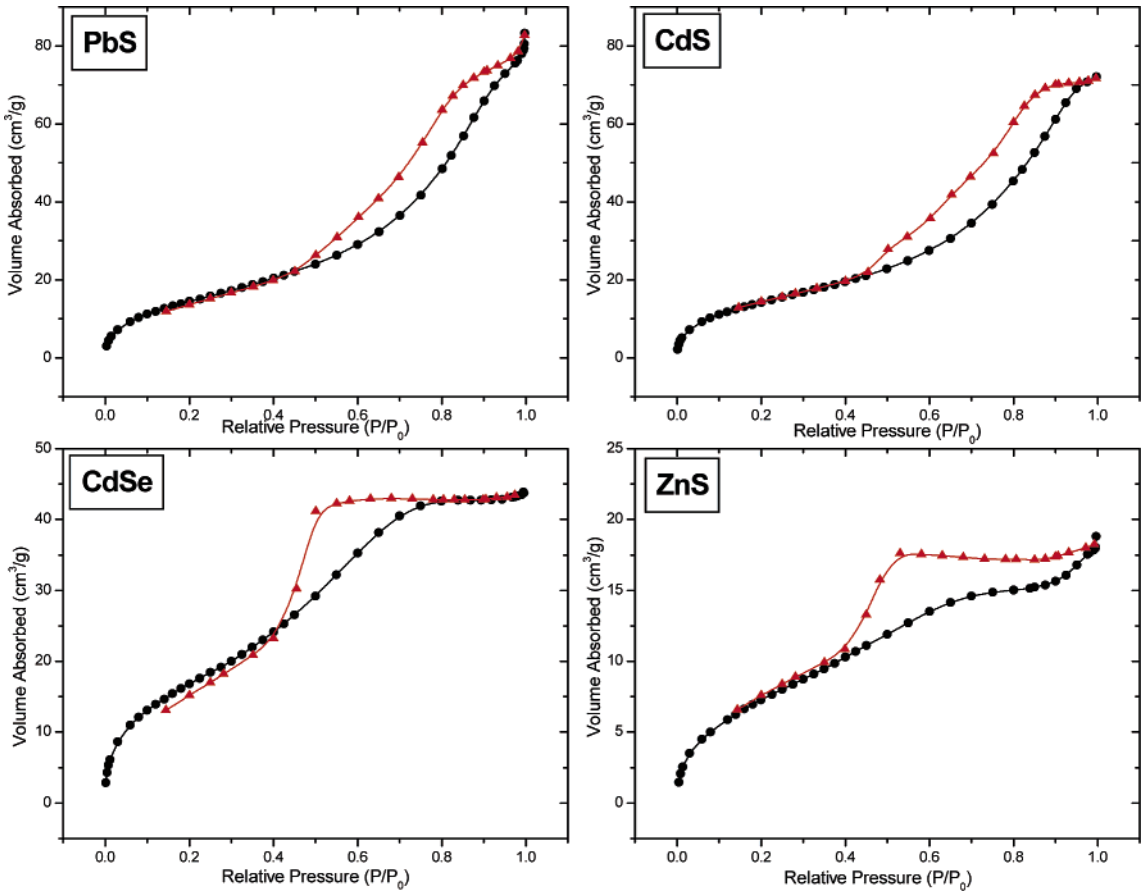

Figure 3. Surface area nitrogen adsorption (●, black) and desorption (▲, red) isotherm analysis of PbS, CdSe, CdS, and ZnS xerogels. The samples were degassed at 100 °C over 48 h prior to analysis.

Table 3. Bulk Band Gap Values, Absorption Onsets of Xerogel Samples, and Crystallite Sizes[a] for the As-Prepared and 100 °C Annealed Xerogels

		as-prepared xerogel		annealed at 100 °C	
xerogel	band gap of the bulk (eV)	band edge	crystallite size[b] (nm)	band edge	crystallite size[b] (nm)
PbS	0.37	0.76	2.6	0.69	3.2
CdSe	1.74	1.96	2.1	1.75	2.2
CdS	2.45	2.31	2.4	2.16	2.5
ZnS	3.70	3.77	1.8	3.75	1.9

[a] Calculated from PXRD data by use of the Scherrer equation. [b] Values obtained from evaluation of the (111) peak in the PXRD pattern.

gesting the extent of quantum confinement is decreased. Representative data from typical samples are shown in Table 3. In general, the observed band-gap for the xerogels remains larger than the single-crystal value. The exception is CdS xerogels, which have an onset of 2.31 eV, smaller than that reported for the single crystal (2.45 eV). This may be attributed to crystalline defects inherent in the individual, low-temperature processed nanoparticles, decreasing the effective band gap for the sample. Indeed, a bulk precipitate of our CdS nanoparticle precursor demonstrates a band gap of 2.05 eV, consistent with this analysis. Hence, the resulting xerogel networks can still be described as a quantum-confined network.

The fact that the transformation of the wet gel to the xerogel results in such a large optical change can be attributed to densification of the aggregate network. Since the particles are physically bonded to each other (there is no intervening ligand shell), the extent of quantum confinement is intimately related to the primary particle size and the dimensionality of the network (the number of connection sites) as well as the quality of the interface between particles. Small-angle X-ray scattering (SAXS) conducted during CdS gelation reveals a mass fractal dimensionality of 1.9,[24] which can be expected to increase upon compaction of the gel body. Hence, the pore collapse during the drying of the xerogel leads to a red shift in the optical absorption of the quantum dot network. The low-temperature process is not amenable to further crystallization of the individual particles or particle aggregates, so the average crystallite size remains essentially unchanged.

The effect of temperature processing of the xerogels was probed by annealing the as-prepared xerogels at 100 °C under active vacuum. The average crystallite sizes increased slightly relative to as-prepared xerogels, whereas the band-edge absorption energies decreased (Table 3). These data are consistent with growth/crystallization of the primary nanoparticle components upon annealing and/or coarsening of the xerogel framework, further reducing the extent of quantum confinement. In the case of ZnS, a small amount of ZnO was observed as an impurity in the PXRD pattern of annealed

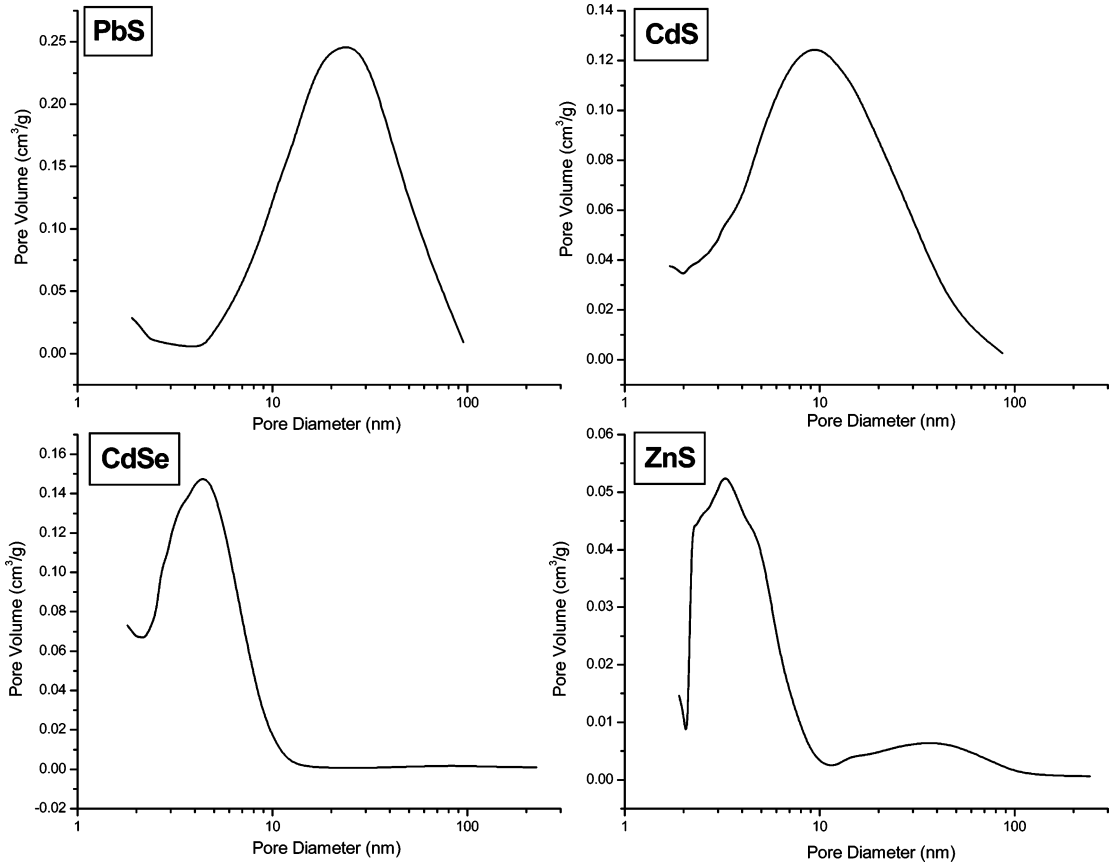

Figure 4. BJH adsorption average pore size distributions for PbS, CdSe, CdS, and ZnS xerogels.

Table 4. BET Surface Area and BJH Average Pore Diameter of Xerogels[a]

sample	BET surface area (m^2/g)	silica equivalence BET surface area[b] (m^2/g)	BJH adsorption average pore diameter (nm)	BJH adsorption cumulative pore volume (cm^3/g)
PbS xerogel	48−57	191−227	7−15	0.12−0.18
CdSe xerogel	41−65	131−207	4−5	0.05−0.07
CdS xerogel	38−55	91−132	5−7	0.05−0.11
ZnS xerogel	29−31	47−50	3−4	0.02−0.03

[a] Two independent samples were evaluated for each system. [b] Silica equivalence values were calculated on a per mole of SiO_2 basis.

samples, also manifested as a small hump at 3.45 eV in the optical band-gap measurements [E_g (ZnO) = 3.4 eV[56]]. The formation of ZnO is attributed to the presence of adventitious oxygen or the transformation of hydroxyl moieties (present on the xerogel surface as a byproduct of hydrogen peroxide oxidation of surface thiolates[24]) to oxide upon heating.

Surface area and porosimetry information were obtained by analysis of nitrogen adsorption/desorption isotherms for PbS, CdSe, CdS, and ZnS xerogels degassed at 100 °C. Figure 3 shows the typical isotherms obtained, whereas the Brunauer−Emmett−Teller (BET) surface areas, Barrett−Joyner−Halenda (BJH) average pore diameters, and BJH cumulative pore volumes are listed in Table 4. Generally, the surface areas are in the range 29−65 m^2/g. When normalized relative to silica on a per-mole basis, these are roughly equivalent to 50−230 m^2/g of silica. This is considerably lower than what can be obtained in the best silica xerogels (500−900 m^2/g), where the synthesis has had the benefit of optimization over decades.[57]

All the isotherms can be described as corresponding to a type IV curve, which is characteristic of a mesoporous material.[58,59] The hysteresis loops observed in the isotherms are indicative of the pore geometry in the material. CdSe and ZnS exhibit an H2-type loop suggestive of "ink-bottleneck" shaped pores,[58] whereas PbS and CdS display a combination of H2 and H3 types, indicating the presence of both "ink-bottleneck" and "slit" pore geometries. In addition, PbS xerogels exhibit a sharp upturn at high partial pressure indicative of liquid condensation associated with the presence of large (macroscopic, >50 nm) pores.

The differences noted in the nitrogen adsorption/desorption isotherms between the PbS and CdS xerogels and those of CdSe and ZnS are also reflected in the BJH modeled pore size distributions (Figure 4). PbS and CdS both have relatively broad distributions extending out to 100 nm (mesoporous−macroporous region), whereas the pores are largely limited to <10 nm in diameter (lower mesoporous region) for the corresponding CdSe and ZnS xerogels.

(56) West, A. R. *Basic Solid State Chemistry*, 2nd ed.; John Wiley: Chichester (England), 1999.
(57) Brinker, C. J.; Scherer, G. W. *Sol−Gel Science*. Academic Press: San Diego, CA, 1990.
(58) Gregg, S. J.; Sing, K. S. W. *Adsorption, Surface Area and Porosity*, 2nd ed.; Academic: New York, 1982.
(59) Webb, P. A.; Orr, C. *Analytical Methods in Fine Particle Technology*; Micromeritics Instrument Corp.: Norcross, GA, 1997.

Table 5. Comparison of Band-Edge Data for Samples of CdSe[a]

	nanoparticles	wet gel	aerogel	xerogel	xerogel (100 °C)	single crystal
band edge (eV)	2.40	2.40	2.20	1.96	1.75	1.74

[a] With dimensionality increasing from 0-D (ca. 4.4 nm particles) to 3-D (single crystal).

Additionally, ZnS xerogels appear to have a second distribution of pores corresponding to the diameter range 10−100 nm. The average pore sizes (Table 4) are in the 3−7 nm range for CdSe, CdS, and ZnS, whereas PbS has a larger pore diameter of 7−15 nm, which correlates with a higher relative surface area (normalized to silica) and a higher cumulative pore volume than the other xerogels. Since the BJH model assumes a cylindrical pore geometry, we have also used density functional theory (DFT), presuming a slit-pore geometry, to model the data. The resulting distributions are similar to those obtained from the BJH model in all cases (Supporting Information), suggesting that the differences observed between the various systems are not merely artifacts of the modeling method. The origin of the differences observed between PbS, CdS and CdSe, ZnS xerogels is unclear but is likely related to the chemical composition in each system, impacting parameters such as the strength of solvent−gel interactions and sticking probabilities for aggregating particles. Nevertheless, the fact that mesoporosity is retained in all the materials suggests they will be suitable for applications that depend on molecular transport.

Effect of Dimensionality on Quantum Confinement: Comparison of Xerogels and Aerogels. The influence of the drying method on the porosity, optical properties, and thermal stability of colloidal networks can be assessed by comparing the benchtop-dried xerogels with supercritically dried aerogels. Benchtop drying is simpler and more amenable to thin-film processing but results in significant volume loss due to pore collapse. In contrast, the absence of a liquid−gas-phase boundary in the supercritical fluid means that the pores can be emptied without catastrophic collapse due to capillary forces. Consequently, the metal chalcogenide aerogels exhibit much larger surface areas of 100−250 m^2/g and greater BJH average pore diameters of 15−45 nm than the xerogels presented here.[22,23] The lower dimensionality of the aerogel framework is more resistant to aggregation and coarsening upon heating, resulting in only a 0.08 eV shift in band gap for CdS upon heating to 100 °C (a 3% change),[22,23] whereas the corresponding xerogel gap decreases by 0.15 eV (a 6.5% change). These data suggest that, for a fractal network composed of discrete nanoparticles of a given size, the extent of quantum confinement is governed by the dimensionality of the network. Thus, upon going from nanoparticles, to wet gel, aerogel, xerogel, and xerogel annealed at 100 °C, there is a steady decrease in band-edge that correlates to increased densification of the networks, with bulklike behavior observed for the annealed xerogel, as demonstrated for CdSe in Table 5. The band-edge observed in gel framework materials naturally also depends on the primary particle size. For example, larger CdSe nanoparticles prepared by use of $W = 3$ material [band onset = 2.24 eV, diameter (mass approximation) = 5.01 nm] produce an aerogel with a band edge of 1.94 eV, similar to that for the xerogels obtained from $W = 2$ CdSe nanoparticles as presented here (1.96 eV). Thus, by adjusting the primary particle size and drying and postannealing conditions, the optical and porosity characteristics of metal chalcogenide gels can be optimized.

Acknowledgment. This work is supported by the National Science Foundation IGERT (DEG-9870720) and CAREER (DMR-0094273) awards and Research Corporation (Research Innovation Award-R10617). We thank Professor Mercouri Kanatzidis (Michigan State University) for the use of solid-state optical band gap equipment.

Supporting Information Available: DFT pore size distribution plots for xerogels of CdS, CdSe, PbS, and ZnS. This material is available free of charge via the Internet at http://pubs.acs.org.

CM0518325